

NUCLEAR PROPERTIES OF A SAMPLE OF NEARBY SPIRAL GALAXIES FROM HUBBLE SPACE TELESCOPE STIS IMAGING¹

C. SCARLATA,^{2,3} M. STIAVELLI,³ M. A. HUGHES,⁴ D. AXON,^{4,5} A. ALONSO-HERRERO,⁶ J. ATKINSON,⁴ D. BATCHELDOR,⁴
J. BINNEY,⁷ A. CAPETTI,⁸ C. M. CAROLLO,⁹ L. DRESSEL,³ J. GERSSEN,³ D. MACCHETTO,³ W. MACIEJEWSKI,¹⁰
A. MARCONI,¹⁰ M. MERRIFIELD,¹¹ M. RUIZ,⁴ W. SPARKS,³ Z. TVETANOV,¹² AND R. P. VAN DER MAREL³

Received 2003 August 5; accepted 2004 June 3

ABSTRACT

We present surface photometry for the central regions of a sample of 48 spiral galaxies (mostly unbarred and barred of type Sbc or Sc) observed with the Space Telescope Imaging Spectrograph on board the *Hubble Space Telescope*. Surface brightness profiles (SBPs) were derived and modeled with a Nuker law. We also analyzed archival Wide Field Planetary Camera 2 images with a larger field of view, which are available for 18 galaxies in our sample. We modeled the extracted bulge SBPs with an exponential, an $r^{1/4}$, or an r^n profile. In agreement with previous studies, we find that bulges of Sbc galaxies fall into two categories: bulges well described by an exponential profile and those well described by an $r^{1/4}$ profile. Only one galaxy requires the use of a more general Sérsic profile to properly describe the bulge. Nuclear photometrically distinct components are found in $\sim 55\%$ of the galaxies. For those that we classify as star clusters on the basis of their resolved extent, we find absolute magnitudes that are brighter on average than those previously identified in spiral galaxies. This might be due to a bias in our sample toward star-forming galaxies, combined with a trend for star-forming galaxies to host brighter central clusters.

Key words: galaxies: bulges — galaxies: nuclei — galaxies: spiral — galaxies: structure

1. INTRODUCTION

This article is part of a series of papers presenting the results of our *Hubble Space Telescope* (HST) program GO-8228 (PI: D. Axon), executed with the Space Telescope Imaging Spectrograph (STIS). The goal of the program is to study the black hole (BH) mass distribution in spiral galaxies.

Studies of the centers of nearby early-type galaxies (elliptical and lenticular galaxies) have revealed that most contain supermassive black holes (see Kormendy & Gebhardt 2001 for a recent review). These studies also revealed a strong correlation between the mass of the BH (M_{BH}) and the mass (or luminosity) of the host spheroid (M_{sph} ; Magorrian et al. 1998;

Marconi & Hunt 2003). An even tighter correlation was thought to exist between M_{BH} and the mean velocity dispersion (σ) of the bulge measured inside its effective radius (Ferrarese & Merritt 2000; Gebhardt et al. 2000). However, Marconi & Hunt (2003) have recently shown that when considering only galaxies with secure BH detections, the above correlations have similar intrinsic dispersion. In contrast, M_{BH} is unrelated to the properties of galaxy disks. These correlations strongly support the idea that the growth of BHs and the formation of spheroids are closely linked (Silk & Rees 1998; Haehnelt & Kauffmann 2000). However, these results are based on samples strongly biased against late Hubble type galaxies: only $\simeq 20\%$ of the detected BHs are in spiral galaxies (Kormendy & Gebhardt 2001; Merritt & Ferrarese 2001).

There are significant differences between bulges of intermediate- and late-type galaxies and those of early-type spiral galaxies (Kormendy 1993; Carollo et al. 1997, 1998). The former (often referred to as “pseudobulges”) are characterized by exponential surface brightness profiles (SBPs), shallow nuclear cusp slopes (Carollo & Stiavelli 1998), and cold kinematics (Kormendy 1993). In contrast, spheroids of early-type spiral galaxies are better described by a de Vaucouleurs $r^{1/4}$ profile, have steep stellar cusps that increase with decreasing luminosity (Carollo & Stiavelli 1998), and are, in general, more similar to small elliptical galaxies than to exponential bulges. Carollo (1999) suggested that exponential and $r^{1/4}$ bulges have different origins. While it seems reasonable (in light of the observational results) that the former form within the disk as a consequence of the secular evolution of the disk itself (Norman et al. 1996), it is difficult to explain the origin of the $r^{1/4}$ bulges with the same mechanism. Therefore, there is the possibility that the $M_{\text{BH}}-M_{\text{sph}}$ relation for spiral galaxies could be different for the two classes of bulges, mirroring the different formation processes. In order to address this, it is necessary to have access to high spatial resolution spectroscopy (to measure the BH mass) and imaging (to characterize

¹ Based on observations with the NASA/ESA *Hubble Space Telescope*, obtained at the Space Telescope Science Institute, which is operated by the Association of Universities for Research in Astronomy, Inc., under NASA contract NAS 5-26555.

² Dipartimento di Astronomia, Univeristà di Padova, Vicolo dell'Osservatorio 2, I-35122 Padua, Italy.

³ Space Telescope Science Institute, 3700 San Martin Drive, Baltimore, MD 21218.

⁴ Department of Physics, Astronomy and Mathematics, University of Hertfordshire, College Lane, Hatfield AL10 9AB, UK.

⁵ Current address: Department of Physics, Rochester Institute of Technology, 84 Lomb Memorial Drive, Rochester, NY 14623-5603.

⁶ Steward Observatory, University of Arizona, 933 North Cherry Avenue, Tucson, AZ 85721.

⁷ Theoretical Physics, Oxford University, Keble Road, Oxford OX1 3NP, UK.

⁸ Osservatorio Astronomico di Torino, INAF, Strada Osservatorio 20, I-10025 Pino Torinese, Italy.

⁹ Departement Physik, HPF G4.3, ETH Hönggerberg, CH-8093 Zurich, Switzerland.

¹⁰ Osservatorio Astrofisico di Arcetri, INAF, Largo Enrico Fermi 5, I-50125 Florence, Italy.

¹¹ School of Physics and Astronomy, University of Nottingham, Nottingham NG7 2RD, UK.

¹² Center for Astrophysical Sciences, Johns Hopkins University, 3400 North Charles Street, Baltimore, MD 21218.

the nuclear SBP). The observing program we are conducting is ideal for these kinds of studies. In fact, the BH mass is derived by modeling the gas kinematics, and the nuclear properties of the bulges are derived by analyzing the high spatial resolution images that were taken to accurately center the galaxy nucleus in the slit.

In this paper we present the STIS images obtained during our *HST* program. We use these data, together with archival *HST* Wide Field Planetary Camera 2 (WFPC2) data available for some of the galaxies, to describe the nuclear and bulge properties of the galaxies in the sample. The paper is organized as follows: The data, the data reduction, and the extraction of the radial SBPs are described in § 2. In § 3 we discuss the radial profile fits used to derive the nuclear slope and bulge type. The principal results concerning the nuclear slopes and galaxy types are presented and discussed in § 3.3. In § 4 we discuss the identification of nuclear star clusters, and we derive their main properties such as size and total magnitude. Lastly, in § 5 we discuss the results.

In Paper I (Marconi et al. 2003) we presented a detailed description of the modeling techniques used to determine the BH mass from the STIS data. The model was then applied to the images and spectra for NGC 4041, the first galaxy to be observed in the *HST* program. In Paper II (Hughes et al. 2003) we presented the STIS spectra, most of the STIS images, and color maps when archival near-infrared NICMOS images were available. In Paper IV (Hughes et al. 2004) we use both color information and the spectra to investigate the ages of the central stellar population. The present paper is Paper III in the series.

2. OBSERVATIONS AND DATA REDUCTION

The galaxy sample observed with STIS consists of 54 spiral galaxies, mostly classified as Sbc and Sc. The galaxies were extracted from a larger sample (128 objects) for which we obtained ground-based $H\alpha$ rotation curves at a seeing-limited resolution of $1''$. VLA radio maps and ground-based R - and B -band CCD images are also available for all the galaxies. The 54 galaxies were chosen to have recession velocities less than 2000 km s^{-1} (in order to be able to resolve the rotation curves within the central few parsecs) and to show emission lines in the nucleus.

The sample galaxies together with their main properties are listed in Table 1. Columns (2) and (3) list the morphological classification and the apparent total B magnitude from the Third Reference Catalogue of Bright Galaxies (RC3; de Vaucouleurs et al. 1991). The Galactic R -band extinction, the distance, and the physical pixel scale are presented in columns (4)–(6), respectively. The last column of Table 1 gives a brief description of the nuclear morphology of the galaxies. Throughout this paper we adopt $H_0 = 65 \text{ km s}^{-1} \text{ Mpc}^{-1}$.

2.1. STIS Data

The STIS images were taken as part of the acquisition procedure in order to accurately center the STIS slit on the galaxy nuclei. They were obtained between 1999 July and 2001 February. We adopted the STIS diffuse-source acquisition procedure (see the STIS Instrument Handbook for details; Proffitt et al. 2002). During the acquisition two $5'' \times 5''$ images were obtained with the optical long-pass filter F28X50LP. After the first image was created from a pair of exposures (see chap. 8 of the STIS Instrument Handbook for details), the position of the target was computed by finding the flux-weighted centroid of the pixels in the brightest checkbox (size

7 pixels), and a second exposure was made from a second pair of exposures with the galaxy nucleus centered in the acquisition aperture. For NGC 134, 3521, 3972, 4389, 5577, and 5713, the slit was not correctly placed on the nucleus of the galaxy. These galaxies are indicated with the word “missed” in Table 1. In these cases, either the centering algorithm did not work properly, or our coordinates of the targets were insufficiently accurate. The pixel scale of the images is $0''.05 \text{ pixel}^{-1}$.

All the images were reduced using the most updated reference files. The raw images were flat-field-corrected using the task BASIC2D in the package STSDAS in IRAF.¹³ The processing done by the flight software is rudimentary; in particular, a single predefined bias value of 1510 DN is subtracted. This value is an approximation of the actual bias, which has been observed to increase with time. (By the end of 2000 the actual level in the acquisition subarray was $1517.3 \pm 1.7 \text{ DN}$.) Since our observations cover a period of time that goes from 1999 July to 2001 February, it is necessary to correct for this effect. We have therefore retrieved from the *HST* archive all bias images taken as part of the STIS CCD Performance Monitor program from 1998 June to 2001 May. The bias level variation as a function of time was fitted with a linear function, and each galaxy image was corrected accordingly.

The two images of the target were aligned and then averaged with simultaneous rejection of residual cosmic rays not removed by the onboard processing of the pairs of exposures. The shifts were computed from the position of the center of the galaxy and any star clusters or point sources visible in the two exposures. For two objects (namely, NGC 3003 and NGC 4088), only the second exposure contained useful data. For these objects, the analysis was performed on the single second exposure. Residual cosmic-ray rejection, for these exposures, was performed with the IRAF task CRMEDIAN.

In order to facilitate the comparison between our results and those of other studies, we calibrated the F28X50LP magnitudes to Cousins R . The photometric zero point was computed using the package SYNPHOT in STSDAS, using different galaxy templates (Kinney et al. 1996). We found that the zero points derived for spiral galaxy templates (Sb and Sc templates) do not show significant differences from each other ($<2\%$), while the zero point computed for the elliptical galaxy template differed more than 5% from the others. Since we do not have color information for the nuclear region of the observed galaxies and since the entire sample mostly consists of Sbc type galaxies, we decided to adopt the calibration computed for the Sb template. All the magnitudes were expressed in VEGAMAG (the spectrum of the star Vega is used as zero point) and were corrected for Galactic extinction following Schlegel et al. (1998). In order to convert from VEGAMAG to ABMAG (a magnitude system with zero point based on a spectrum with constant flux per unit frequency; Oke 1974), the transformation for an Sb galaxy spectral template is $m_{R,\text{Vega}} = m_{R,\text{AB}} - 0.21$. In Figure 1 we present the reduced images of the galaxies. The nucleus is not always at the center of the field, because the images are a mosaic of two exposures.

2.2. WFPC2 Data

The field of view of the STIS images is only $5'' \times 5''$, which in physical units translates to between $0.2 \text{ kpc} \times 0.2 \text{ kpc}$ and $0.7 \text{ kpc} \times 0.7 \text{ kpc}$, depending on the distance of the galaxy.

¹³ IRAF is distributed by the National Optical Astronomy Observatory, which is operated by the Association of Universities for Research in Astronomy, Inc., under cooperative agreement with the National Science Foundation.

TABLE 1
GALAXY SAMPLE

Name (1)	Type (2)	m_B (mag) (3)	A_R (mag) (4)	D (Mpc) (5)	Scale (pc pixel ⁻¹) (6)	Comments (7)
NGC 134.....	.SXS4./SBbc	11.25	0.048	24.49	5.93	Missed
NGC 157.....	.SXT4./SBbc	11.05	0.119	27.64	6.70	Strong dust lane across the center
NGC 255.....	.SXT4./SBbc	12.31	0.071	26.30	6.37	Bright knots spread over the entire galaxy, the brightest is not at the center of the external isophotes
NGC 289.....	.SBT4./SBbc	11.79	0.052	25.32	6.14	Dust on the plane of the disk, the SBP keeps rising until the <i>HST</i> resolution
NGC 613.....	.SBT4./SBbc	10.99	0.052	22.98	5.57	Disturbed morphology, dust lanes and bright knots; nuclear dust ring at 0''25 from the nucleus
NGC 1255.....	.SXT4./SBbc	11.68	0.037	25.49	6.18	Regular morphology
NGC 1300.....	.SBT4./SBbc	11.22	0.081	24.10	5.84	Regular morphology, spiral-like dust lanes down to the center
NGC 1832.....	.SBR4./SBbc	12.12	0.195	28.63	6.94	Spiral arms down to the center, wrapping around the nucleus
NGC 2748.....	.SA.4./Sbc	12.41	0.071	25.68	6.22	Asymmetric morphology due to diffuse dust lanes, nucleus not well defined
NGC 2903.....	.SXT4./SBbc	9.56	0.083	7.34	1.78	Spiral arms down to the center, many star-forming bright knots
NGC 2964.....	.SXR4*/SBbc	12.26	0.052	19.92	4.83	Dust lanes and bright knots
NGC 3003.....	.S.4\$/SBbc	12.41	0.036	22.47	5.44	A clear center is not present, bright knots
NGC 3021.....	.SAT4*/Sbc	12.60	0.036	23.42	5.67	Dusty spiral arms down to the center, bright central nucleus, possibly a nuclear bar
NGC 3162.....	.SXT4./SBc	12.38	0.062	18.77	4.55	Wrapped spiral arm, or nuclear ring
NGC 3254.....	.SAS4./Sbc	12.62	0.039	20.08	4.87	Narrow dust lane close to the nucleus, smooth underlying surface brightness
NGC 3259.....	.SXT4*/SBbc	12.90	0.039	27.98	6.78	Smooth surface brightness
NGC 3310.....	.SXR4P/SBbc	11.08	0.060	16.48	3.99	Strong dust lane crossing the center of the galaxy
NGC 3403.....	.SA.4*/Sbc	13.08	0.277	22.08	5.35	Flocculent spiral arms, knots of star formation, resolved component
NGC 3521.....	.SXT4./SBbc	9.73	0.155	9.46	2.29	Missed
NGC 3642.....	.SAR4*/Sbc	11.67	0.029	26.10	6.32	Dusty spiral arms, elongated nuclear structure, probably due to a dust lane close to the center
NGC 3684.....	.SAT4./Sbc	12.27	0.069	16.20	3.92	Disturbed morphology, strong dust lanes, many bright knots of star formation
NGC 3686.....	.SBS4./SBbc	11.96	0.065	16.10	3.90	Bright central component, resolved
NGC 3756.....	.SXT4./SBbc	12.33	0.031	21.17	5.13	Dusty spiral arms
NGC 3887.....	.SBR4./SBbc	11.42	0.092	14.79	3.58	Dust lanes defining tightly wrapped spiral arms, hints of a nuclear bar
NGC 3949.....	.SAS4*/Sbc	11.70	0.057	13.17	3.19	Dust lanes
NGC 3953.....	.SBR4./SBbc	10.85	0.080	17.41	4.22	Dust lane passing close to the nucleus
NGC 3972.....	.SAS4./SBbc	12.99	0.037	14.45	3.50	Missed
NGC 4030.....	.SAS4./Sbc	11.67	0.071	19.61	4.75	Flocculent spiral arms
NGC 4041.....	.SAT4*/Sbc	11.85	0.047	20.85	5.05	Flocculent spiral arms down to the center
NGC 4051.....	.SXT4./SBbc	10.90	0.035	11.53	2.79	Very bright central component
NGC 4088.....	.SXT4./SBc	11.16	0.053	12.74	3.09	Flocculent spiral arms, nucleus obscured by dust
NGC 4100.....	PSAT4./Sbc	11.89	0.062	17.55	4.25	Asymmetric morphology, strong dust obscuration, numerous knots of star formation
NGC 4212.....	.SA.5*/Sc	11.88	0.089	17.50	4.25	Dust absorption down almost to the center
NGC 4258.....	.SXS4./SBbc	9.09	0.043	7.78	1.89	Regular morphology, no visible spiral arms
NGC 4303.....	.SXT4./SBbc	10.18	0.060	21.81	5.28	Small flocculent spiral arms and filaments
NGC 4321.....	.SXS4./SBbc	10.07	0.070	22.69	5.50	Dust absorption on the disk plane, no well-defined spiral arms
NGC 4389.....	.SBT4P*/SBbc	12.59	0.039	11.82	2.86	Missed
NGC 4420.....	.SBR4*/SBc	12.86	0.048	23.45	5.68	No well-defined dust lanes
NGC 4527.....	.SXS4./SBbc	11.45	0.059	24.16	5.85	Severe dust obscuration, nucleus not well defined
NGC 4536.....	.SXT4./SBbc	11.15	0.049	25.24	6.11	Asymmetric structure due to dust obscuration
NGC 5005.....	.SXT4./SBbc	10.74	0.038	14.88	3.60	Nucleus not well defined, dust obscuration
NGC 5054.....	.SAS4./Sbc	11.84	0.220	23.44	5.68	Flocculent and not well defined spiral arms
NGC 5055.....	.SAT4./Sbc	9.30	0.047	8.447	2.05	No visible spiral arms or dust lanes
NGC 5247.....	.SAS4./SBbc	11.17	0.237	17.63	4.27	Patchy dust absorption
NGC 5248.....	.SXT4./SBbc	11.01	0.065	16.12	3.90	Well-defined star-forming spiral arm
NGC 5364.....	.SAT4P/Sbc	11.37	0.073	17.36	4.20	Regular morphology, resolved central cluster
NGC 5577.....	.SAT4*/Sbc	13.74	0.109	21.29	5.16	Missed
NGC 5713.....	.SXT4P/SBbc	11.87	0.105	27.40	6.64	Missed
NGC 5879.....	.SAT4*/Sbc	12.18	0.033	14.29	3.46	Dust lane down to very close to the center
NGC 5921.....	.SBR4./SBbc	11.76	0.107	21.95	5.32	Regular morphology, several spiral arms defined by dust lanes
NGC 6384.....	.SXR4./SBbc	11.61	0.330	26.49	6.42	Regular morphology, weak dust lane
NGC 6951.....	.SXT4./SBbc	11.99	0.978	26.30	6.37	Spiral arms down to the center
NGC 7314.....	.SXT4./SBbc	11.68	0.057	22.92	5.55	Very bright nucleus, smooth surface brightness
NGC 7331.....	.SAS3./Sbc	10.26	0.242	17.16	4.16	Regular morphology, no visible spiral arms

NOTE.—Col. (1): Galaxy name. Col. (2): Morphological classification from the RC3 (de Vaucouleurs et al. 1991, left) and Paturel et al. (2003, right). Col. (3): Total observed blue magnitude from the RC3. Col. (4): The R -band Galactic extinction from Schlegel et al. (1998). Col. (5): Galaxy distance. Col. (6): Image scale in parsecs per STIS pixel. Col. (7): Description of the nuclear morphology of the galaxy.

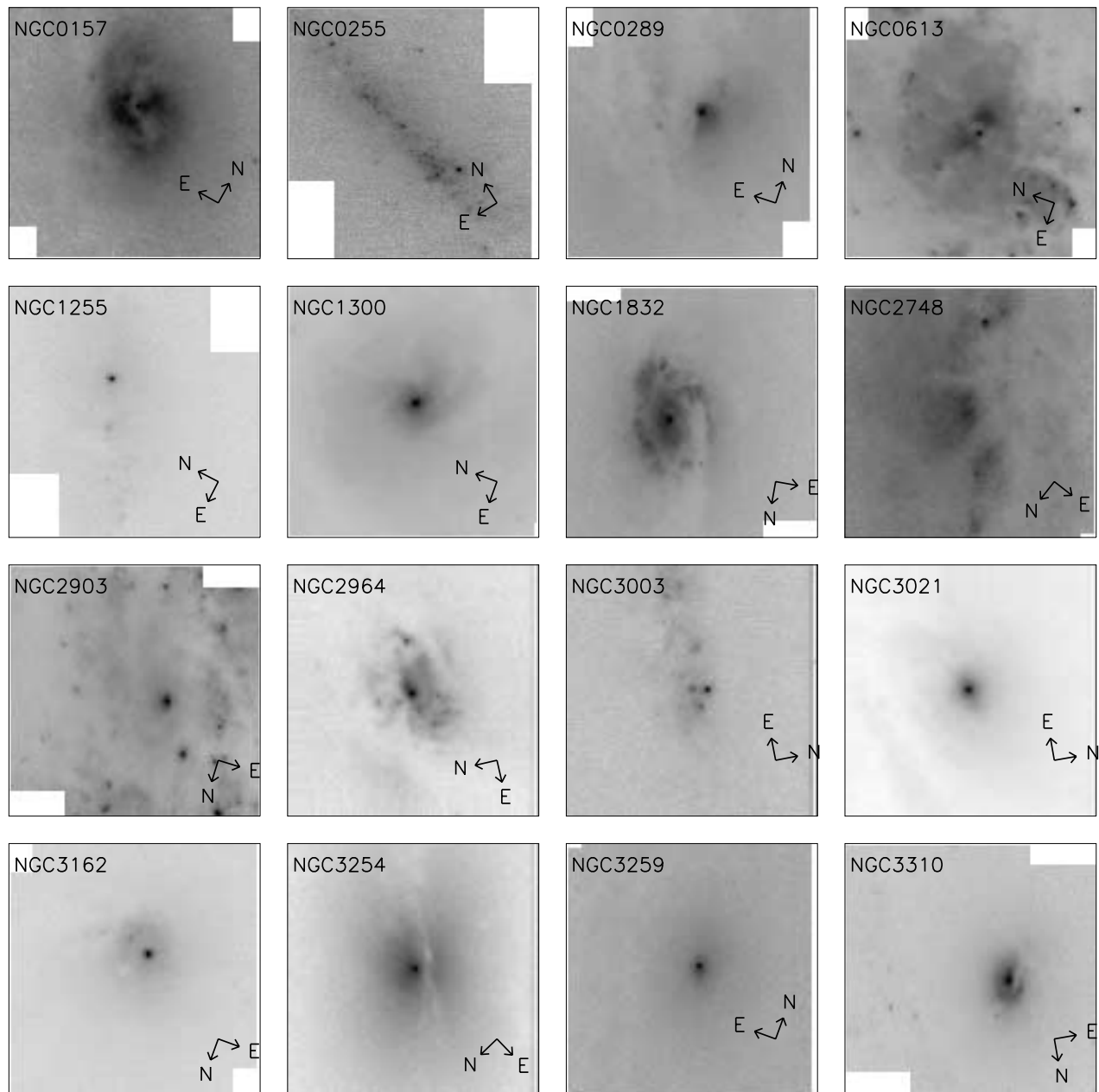


FIG. 1.—F28X50LP images of the galaxies in the sample. The field of view is $\simeq 5'' \times 5''$.

Although this provides important information about the structure of the innermost region, it does not fully cover the bulge and the disk components of the galaxy. For this reason we searched the *HST* archive for WFPC2 images of the sample galaxies. We found data for 18 objects. Most of the galaxies were observed with the filter F606W, three galaxies (NGC 5248, NGC 7314, and NGC 7331) with F814W, and two (NGC 4321 and NGC 4536) with F555W. We retrieved from the *HST* archive the on-the-fly calibrated images that are reprocessed with the most recent reference frames for flat-fielding, bias, and dark current subtraction. The different exposures of the same target were combined and cosmic-ray-cleaned in a single step performed using the IRAF/STSDAS task CRREJ. Absolute photometric calibration was obtained by using the photometric zero points for the filters provided by Holtzman et al. (1995) to facilitate comparison with the results of Carollo & Stiavelli (1998). The magnitude in the F814W filter was then used to

estimate the *V*-band magnitude using SYNPHOT in STSDAS. Since this correction depends on the spectral energy distribution of the object, it was calculated using the Kinney et al. (1996) Sb spectral template. The magnitudes were corrected for Galactic extinction following Schlegel et al. (1998).

2.3. Surface Brightness Profiles

For each galaxy we extracted the surface brightness profile by fitting ellipses to the isophotes using the isophote-fitting program ELLIPSE in IRAF. Before running ELLIPSE on the images, we corrected for the presence of dust lanes, following the technique introduced by Carollo et al. (1997). Briefly, a two-dimensional model of the galaxy was created assuming constant ellipticity and position angle with radius, equal to the values for the outermost isophotes. The difference between the model and the original data gives an image with flux only in the regions of dust absorption. Pixels with significant flux in

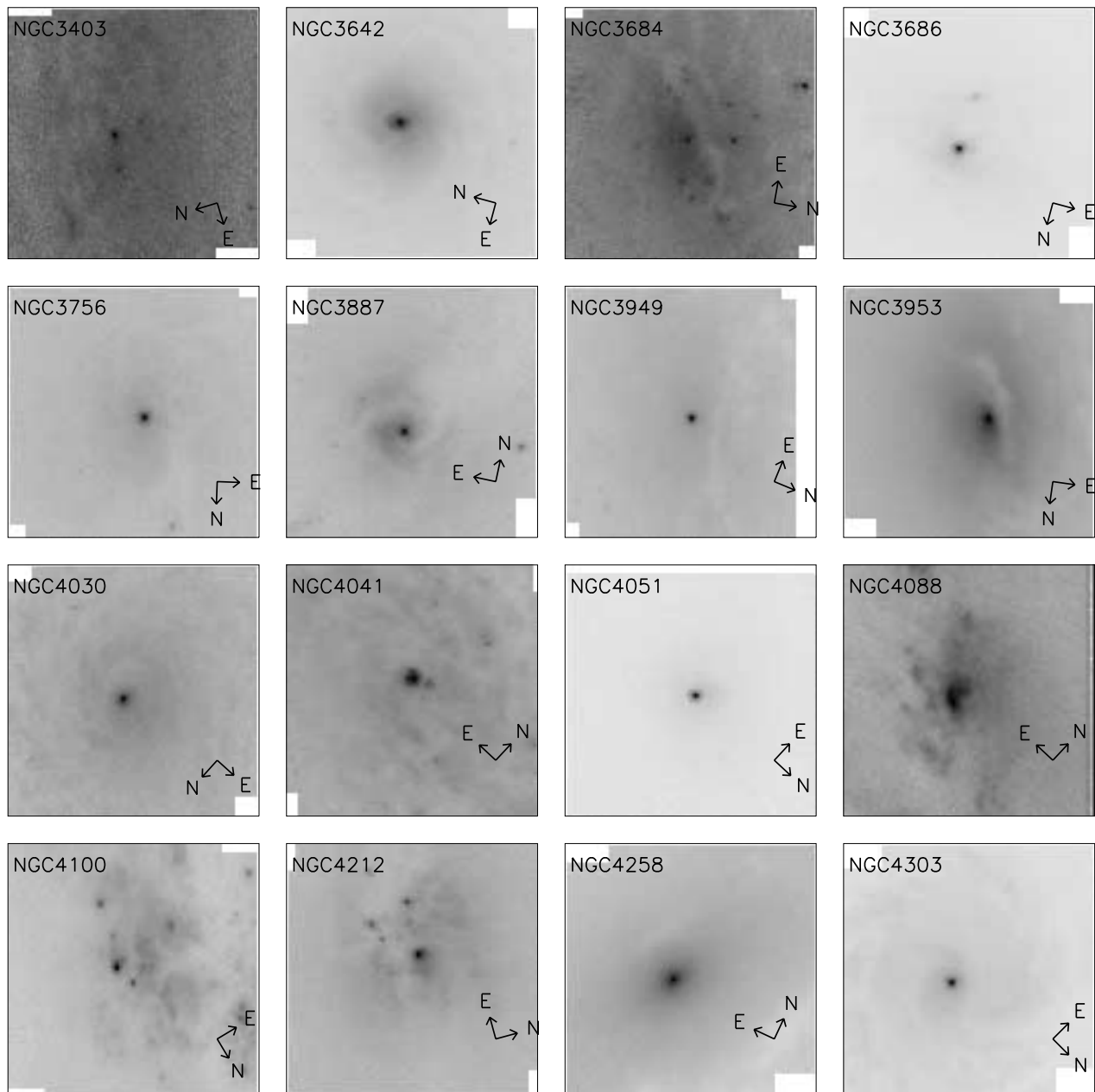


FIG. 1.—Continued

the difference image (above 3σ level) were replaced on the actual image by the model. This procedure was repeated iteratively until convergence was reached. Typically only two or three iterations were needed.

This technique allows us to correct for patchy/filamentary dust absorption and has the advantage of being independent of any physical model of the nature of the dust and its distribution with respect to the stars. It does not correct for any smooth or extended dust component. However, the influence of an extended/diffuse dust component on the structural parameters derived from the SBP fit was studied in detail by Carollo (1999), using optical and infrared data of the nuclear regions of a sample of spiral galaxies. This work showed that the photometric structural parameters derived from optical images, when corrected with the Carollo et al. (1997) algorithm, are accurate and do not suffer significantly from any residual uncorrected dust extinction.

The adopted method can be used to derive an estimate of the extinction in each pixel of the image. Following Witt et al. (1992), we defined the effective optical depth (absorption plus scattering) as $\tau_{\text{eff}} = -\ln(I_{\text{obs}}/I_{\text{mod}})$, where I_{obs} is the observed flux density and I_{mod} is the flux density in the reconstructed two-dimensional model. For most of the galaxies we found that $\simeq 85\%$ of the pixels to which a correction was applied have $\tau_{\text{eff}} < 0.4$. This corresponds to $\tau_{\text{eff},V} < 0.6$. The conversion between τ_{eff} (which is the average over the wavelengths included in the F28X50LP filter) and $\tau_{\text{eff},V}$ was computed by using the spectral template of an Sb galaxy and using the extinction law as given in Cardelli et al. (1989). For these values of the optical depth, the contribution of scattered light to the total emerging light is less than 5% unless particular geometries in the dust/stars distribution are considered.

The extracted *R*-band STIS SBPs for 40 galaxies are presented in Figure 2. For a few of the sample galaxies, the

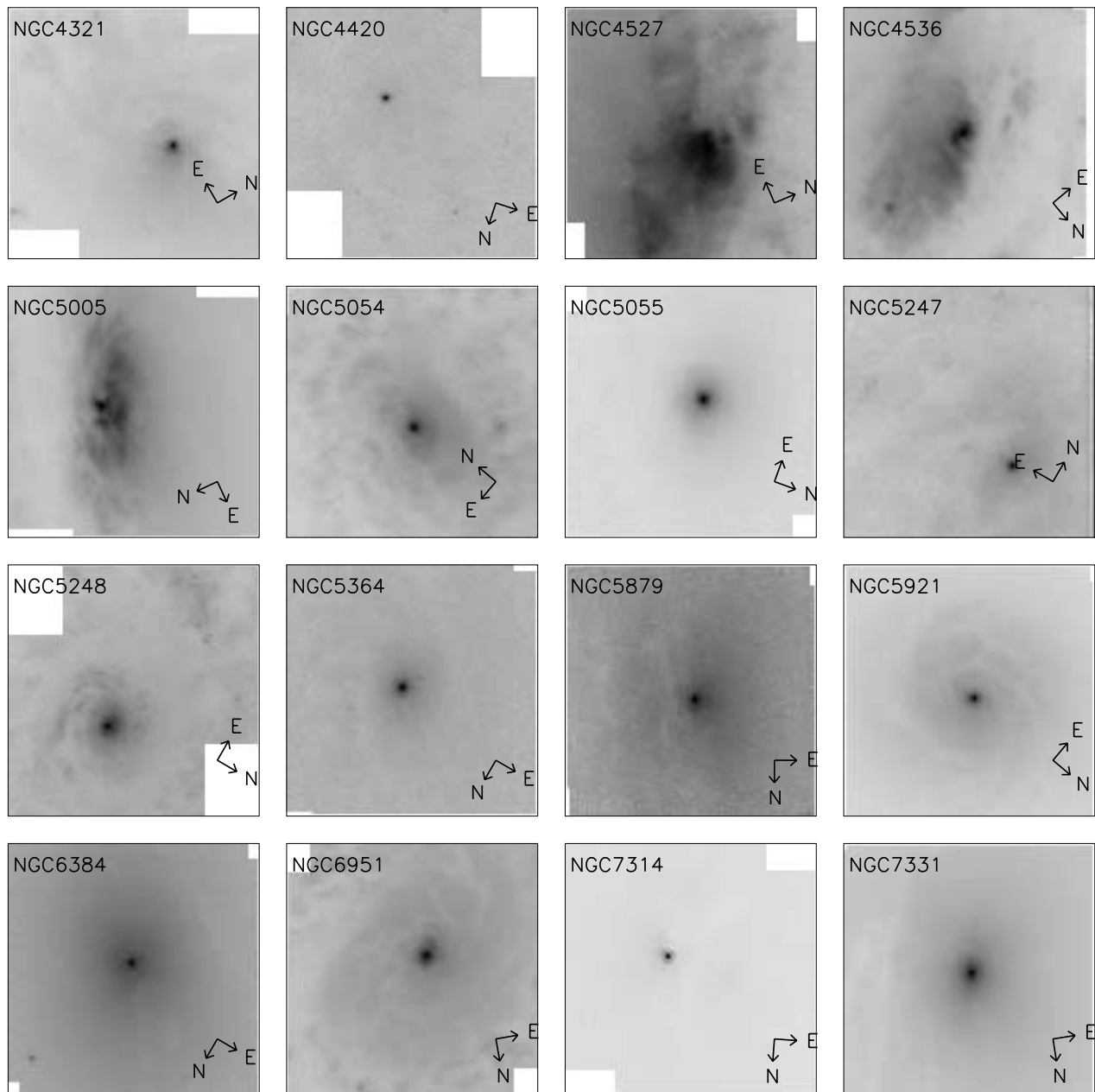


FIG. 1.—Continued

patches and lanes of dust are too prominent (e.g., NGC 4527) to allow a meaningful correction for its effect on the galaxy SBP with the Carollo et al. (1997) algorithm. In a few other galaxies either the presence of bright knots of star formation or a too small gradient in the surface brightness made it impossible to obtain a good description of the galaxy with an elliptical isophote analysis. For these reasons we failed to obtain a meaningful isophotal fit for eight galaxies in the STIS sample and three in the WFPC2 sample. In Figure 3 we present the K -band radial SBPs measured on the WFPC2 images.

3. SURFACE BRIGHTNESS PROFILE MODELING

3.1. Average Logarithmic Slope $\bar{\gamma}$

Since the radial extent of the extracted STIS SBPs is only a few arcseconds, we decided to fit them with a “Nuker law” (Lauer et al. 1995), without trying any decomposition into bulge and disk components in the STIS data. The Nuker law

has been proved to accurately describe the central part of galaxy profiles both for early-type galaxies (Ferrarese et al. 1994; Forbes et al. 1995; Lauer et al. 1995; Ravindranath et al. 2001; Laine et al. 2003) and spiral galaxies (Carollo et al. 1997; Seigar et al. 2002). It assumes that the SBP is a combination of two power laws with different slopes (γ and β) for the inner and the outer regions, respectively. The radius at which the transition between the two power laws occurs is the break radius r_b . The surface brightness at r_b is I_b , and the sharpness of the transition is described by the parameter α . The functional form of the SBP is

$$I(r) = 2^{(\beta-\gamma)/\alpha} I_b \left(\frac{r}{r_b}\right)^{-\gamma} \left[1 + \left(\frac{r}{r_b}\right)^\alpha\right]^{(\gamma-\beta)/\alpha}. \quad (1)$$

In order to derive the parameters describing the galaxy profiles (α , β , γ , I_b , and r_b), we iteratively fitted the SBP

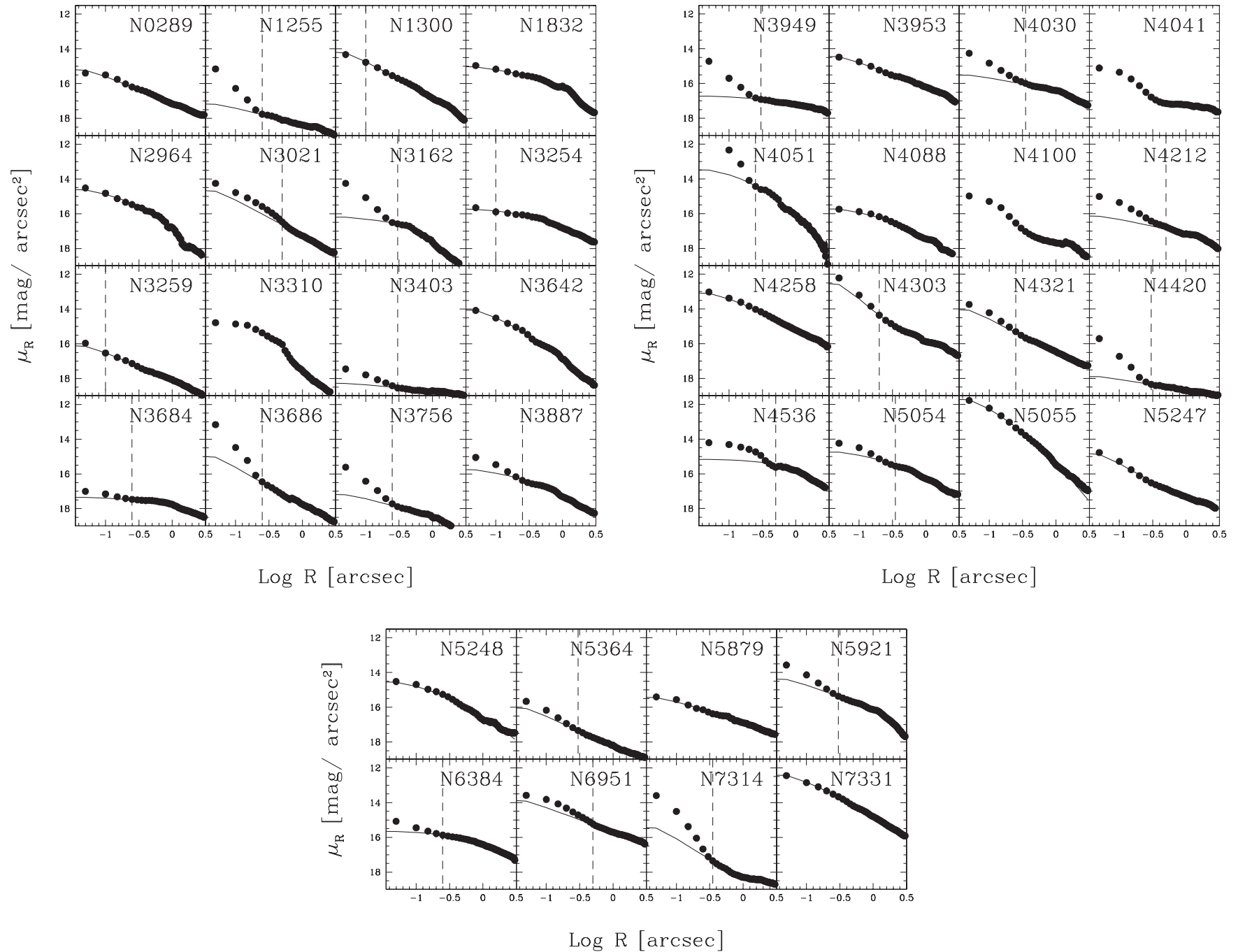


FIG. 2.—The R -band SBPs extracted from the STIS data (circles) and best-fit Nuker-law models (solid lines). The model was convolved with the STIS PSF before plotting. The error bars in the measured galaxy profiles are comparable to the symbol size. Dashed vertical lines indicate the inner radius used in the fit.

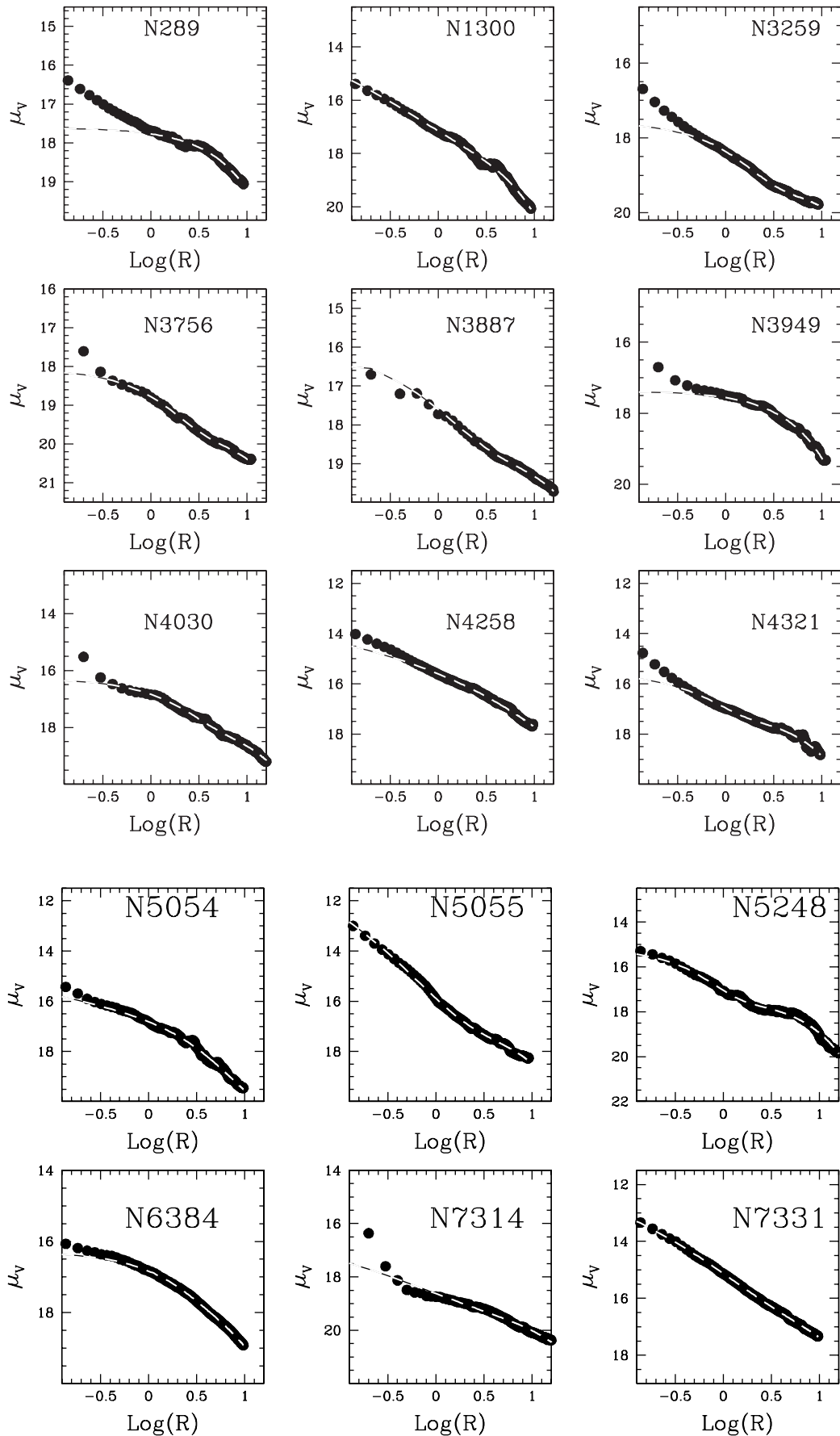


FIG. 3.—The V -band SBPs extracted from the WFPC2 data (circles) and best-fit model from col. (8) of Table 2 (dashed lines). The model was convolved with the WFPC2 PSF before plotting.

model to the observations using a nonlinear χ^2 minimization based on the Levenberg-Marquardt method (e.g., Bevington & Robinson 1992). The fit was done over a user-specified radial range, taking into account the instrumental point-spread function (PSF) by convolving the model profile with the appropriate PSF. The latter was created for the STIS-F28X50LP setup using the Tiny Tim software (Krist & Hook 2001). The convolution was performed in the two-dimensional plane of the sky as a product in the Fourier domain, before the χ^2 minimization. In order to avoid numerical artifacts, the model and the PSF were supersampled by a factor of 5 before the convolution.

The presence of a photometrically distinct nuclear component is one of the main sources of uncertainty in deriving the parameters describing the underlying galaxy light (see, e.g., Carollo et al. 1998). One possible approach is to fit a two-component model to the SBP, with one component describing the nuclear-source profile and the other the underlying galaxy (Böker et al. 2002). Another possibility is to fit the model describing the galaxy only in a region not affected by the nuclear source (Stiavelli et al. 2001). We decided to adopt the second strategy, since we were mainly interested in measuring the central slope of the galaxy SBP. Furthermore, it is not clear which analytical form is convenient to use to describe these nuclear components, since they can be dominated by active galactic nucleus (AGN) light (point-source-like profile), by a star cluster, or by a combination of the two.

The radius r_0 starting from which the SBP was considered unaffected by light coming from the central component was identified by eye for each galaxy's SBP. We typically found r_0 ranging from $0''.3$ to $0''.5$. Since the choice of r_0 is somewhat subjective (being the extent of the central component estimated visually from the profile), it can be a source of errors. We verified that changing the radial range by $\pm 0''.05$ does not significantly alter the values of the Nuker parameters derived in the fit.

The slope of the SBPs for $r \rightarrow 0$ was computed as the mean slope ($\bar{\gamma}$) between $0''.1$ and $0''.5$ of the best-fit model (Stiavelli et al. 2001). Since $\bar{\gamma}$ is computed using the model, it is not affected by either the STIS PSF or light coming from a nuclear component. To verify the latter, we checked whether there was any correlation between the presence of a nuclear source (either resolved or point source) and the value of $\bar{\gamma}$ measured from the model. We divided all galaxies into three classes: no central component, class = 1; point source, class = 2; and resolved component, class = 3. In Figure 4 we plot the measured values of $\bar{\gamma}$ as a function of the object class. It can be seen that there is no correlation between the slope and the presence of a central source, which provides confidence that the adopted strategy for deriving the parameters is correct. For $\sim 80\%$ of the galaxies, the average of the nuclear slope is in agreement with the fitted γ . For the other objects, the fitted value is $\simeq 0$, but this value is not reached at observationally accessible radii, given the accompanying low values of r_b . Therefore, $\bar{\gamma}$ is a more robust description of the galaxy SBP.

The fitted values of the Nuker parameters (α , β , γ , r_b , and I_b) are listed in Table 2, together with the values of the nuclear cusp slope $\bar{\gamma}$. The best-fit profiles (PSF-convolved) are superposed on the data in Figure 2.

Nine galaxies of our sample are also present in the sample of Carollo et al. (2002, hereafter C02), for which Seigar et al. (2002) obtained the average logarithmic slope of the NICMOS (H -band) SBPs, using the same definition used here. They noticed that $\bar{\gamma}$ derived from the visual passband and from the

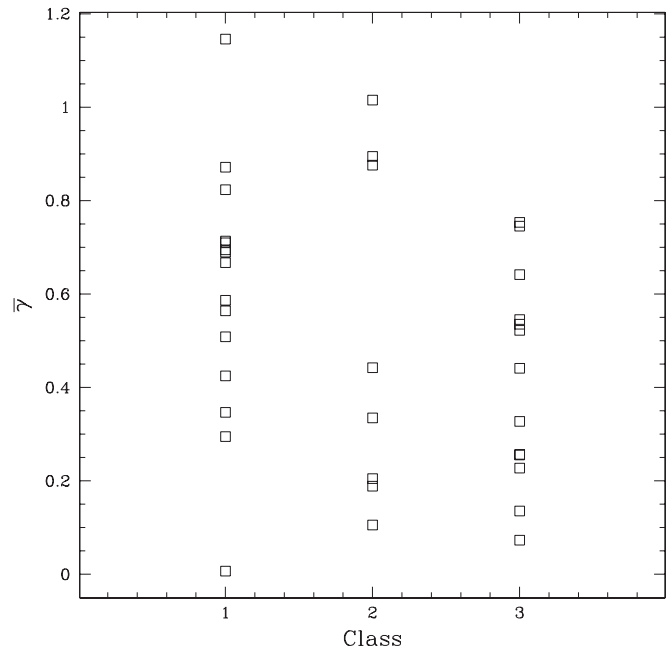


FIG. 4.—Average logarithmic central cusp slope $\bar{\gamma}$ as a function of the class of the object: class = 1, no central component; class = 2, pointlike central component; and class = 3, resolved central component. This figure indicates that there is no correlation between the presence of a nuclear source and the value of $\bar{\gamma}$ measured from the model.

IR data are in good agreement. Hence, it is meaningful to compare our results with theirs. In Figure 5 we show the comparison between the average logarithmic slope computed by Seigar et al. (2002; $\bar{\gamma}_H$) from the NICMOS images and the value ($\bar{\gamma}_R$) computed here for six galaxies. The results agree within the uncertainties. The galaxy (NGC 4536) for which $\bar{\gamma}_R$ and $\bar{\gamma}_H$ are significantly different has a morphology that is strongly affected by dust extinction in the STIS images (see Fig. 1). For three other galaxies in common to our sample (NGC 2784, NGC 2903, and NGC 4527), it was not possible to measure the SBP from our STIS data.

In principle, there need not always be exact agreement between $\bar{\gamma}_R$ and $\bar{\gamma}_H$ if there is a strong color gradient in the nuclear regions of these galaxies due to either a change in age or metallicity of the stellar population or if there are uncorrected residual effects of dust extinction (Witt et al. 1992). However, the fact that a good correlation is observed (Seigar et al. 2002) suggests that these issues are generally not affecting the analysis.

3.2. Analytical Fits to the Bulge Component

We tried to model the more extended WFPC2 SBPs with a variety of analytical profiles. Besides the bulge component, we also took into account the presence of the disk of the galaxy when visible. We used the exponential law to describe the radial SBP of the disk component (Freeman 1970). For the bulge component we used (1) a single exponential, (2) a de Vaucouleurs ($r^{1/4}$), and (3) a Sérsic (r^n ; Sérsic 1968) profile. The program used to fit the profile was similar to the one used to fit the Nuker law. The WFPC2 PSF was created for the different setups and different positions on the chip that were used, using the Tiny Tim software (Krist & Hook 2001). It was convolved with the model before the fit. To determine the nature of the bulge, we fitted the profiles only for radii greater than $1''$. This ensures that the two regions used to measure the

TABLE 2
RESULTS OF SBP FITS

Name (1)	$\bar{\gamma}$ (2)	α (3)	β (4)	γ (5)	r_b (arcsec) (6)	I_b (R-band) (mag arcsec ⁻²) (7)	Bulge ($r > 1''$) (8)	$r_{0,\text{bulge}}$ (arcsec) (9)	$m_{V,\text{bulge}}$ (mag) (10)	Sérsic n ($r > 1''$) (11)
NGC 289.....	0.61	0.00	0.72	0.56	1.09	17.17	Expo.	6.73	11.47	1.33
NGC 1255.....	0.39	17.87	0.46	0.41	1.26	18.48
NGC 1300.....	0.81	37.59	1.50	0.85	1.91	17.40	$r^{1/4}$	3.94	14.3	0.34
NGC 1832.....	0.35	1.68	3.15	0.29	2.36	17.40
NGC 2964.....	0.68	1.42	1.94	0.40	0.68	16.35	NGF
NGC 3021.....	0.82	0.01	0.80	0.91	0.93	17.20
NGC 3162.....	0.30	5.92	1.27	0.22	0.47	16.77
NGC 3254.....	0.33	0.71	1.35	0.00	1.17	16.88
NGC 3259.....	0.64	0.58	0.67	0.67	1.08	18.17	Expo.	0.97	15.89	0.81
NGC 3403.....	0.15	0.63	0.18	0.15	2.18	18.87
NGC 3642.....	0.89	0.92	1.58	0.60	0.53	16.06
NGC 3684.....	0.09	11.17	0.59	0.10	0.74	17.62
NGC 3686.....	0.86	0.38	0.55	1.14	0.60	17.29
NGC 3756.....	0.41	11.22	0.89	0.43	1.11	18.51	Expo.	1.04	16.26	0.90
NGC 3887.....	0.45	1.91	0.97	0.33	0.53	16.72	r^n	0.49	16.48	0.55
NGC 3949.....	0.16	0.87	0.41	0.00	0.38	16.95	Expo.	5.74	11.58	0.72
NGC 3953.....	0.57	8.02	3.29	0.59	2.75	17.10
NGC 4030.....	0.29	145.71	0.79	0.30	1.15	16.44	Expo.	2.00	13.94	0.96
NGC 4051.....	0.82	0.61	3.65	0.05	1.90	17.26
NGC 4088.....	0.54	0.51	1.78	0.00	1.08	17.48
NGC 4212.....	0.33	40.54	1.00	0.35	1.64	17.34
NGC 4258.....	0.67	0.27	1.64	0.00	0.70	14.84	$r^{1/4}$	87.56	8.11	0.33
NGC 4303.....	1.06	8.21	0.65	1.28	0.32	14.95
NGC 4321.....	0.76	0.14	0.02	1.39	1.73	16.90	Expo.	0.45	15.59	0.95
NGC 4420.....	0.26	0.11	0.01	0.45	1.38	18.76
NGC 4536.....	0.18	1.09	2.19	0.00	2.34	16.62	NGF
NGC 5054.....	0.48	0.52	1.68	0.03	1.40	16.54	$r^{1/4}$	30.54	10.71	0.30
NGC 5055.....	1.17	0.37	2.96	0.00	0.63	14.62	$r^{1/4}$	1.00	12.84	0.27
NGC 5247.....	0.85	18.05	0.54	0.89	0.52	16.92
NGC 5248.....	0.64	0.48	1.92	0.00	0.92	16.43	Expo.	0.38	15.37	1.02
NGC 5364.....	0.70	1.35	0.33	0.77	1.88	18.63
NGC 5879.....	0.48	0.14	1.06	0.00	0.58	16.57
NGC 5921.....	0.56	8.15	1.62	0.58	1.41	16.43
NGC 6384.....	0.23	0.79	1.60	0.00	2.36	17.02	Expo.	1.38	14.01	0.84
NGC 6951.....	0.58	0.32	0.28	0.79	1.31	15.84	NGF
NGC 7314.....	0.95	17.40	0.31	0.99	0.77	18.16	$r^{1/4}$	22.33	13.56	0.24
NGC 7331.....	0.76	0.21	1.86	0.00	0.98	14.76	$r^{1/4}$	7.62	10.88	0.23

NOTE.—Col. (1): Galaxy name. Col. (2): Average logarithmic slope between $0''1$ and $0''5$. Cols. (3)–(7): Nuker best-fit parameters. The fit was done to the STIS data and excluded the very central pixels if a nuclear component is present. Col. (8): Bulge classification derived from the WFPC2 SBP for $r > 1''$; NGF indicates that no meaningful isophotal fit could be extracted for the galaxy. Col. (9): Bulge scale radius in arcseconds defined as the effective radius of the $r^{1/4}$ model or the scale radius for the exponential bulges. Col. (10): Total apparent V magnitude of the bulge component. Col. (11): Index n of the best-fitting Sérsic model.

nuclear cusp slopes and the bulge properties are independent. In Table 2 we report the bulge classification, the scale radius $r_{0,\text{bulge}}$, the total apparent magnitude $m_{V,\text{bulge}}$, and the Sérsic index n . The best-fit profiles (PSF-convolved) are superposed on the data in Figure 3.

3.3. Results

We were able to measure the Nuker parameters of the nuclear profile for 37 galaxies out of the 40 for which we could extract the SBP. We find that $\simeq 56\%$ of the galaxies have “steep” cusps ($\bar{\gamma} > 0.5$). The same fraction was found by Carollo & Stiavelli (1998) in their total sample of 41 spiral galaxies. They found also that going from early-type (S0a–Sa) to late-type spiral galaxies (Sc–Sd), the fraction of $r^{1/4}$ bulges and the average nuclear slope decrease. Almost all the galaxies in our sample are classified as Sbc in the RC3 (see Table 1). From Figure 5 of Carollo et al. (1998) we deduce that in their sample $\simeq 25\%$ of Sbc galaxies have

$\bar{\gamma} > 0.5$. For our sample (excluding the four Sc galaxies) we find that $\simeq 60\%$ of the Sbc galaxies have $\bar{\gamma} > 0.5$. This difference could be due to the smaller sample of Carollo et al. (they have only 8 Sbc galaxies out of 41 spiral galaxies) compared with our sample (33 Sbc spiral galaxies). Furthermore, the difference between two contiguous morphological classes is somewhat arbitrary and depends on visual inspection of photographic sources. Considering together Hubble types from Sb to Sc in the Carollo et al. sample, the fraction of galaxies with “steep” cusps increases slightly ($\simeq 33\%$) but is still lower than in our sample. Our fraction is more similar to the fraction of “steep” bulges in the classes S0a–Sab ($\simeq 70\%$) in the Carollo et al. sample.

Concerning the bulge properties, we find that eight galaxies host a bulge that is well described by an exponential profile and six are well described by an $r^{1/4}$ profile. We find only one galaxy (NGC 3887) for which the bulge is best described by a more general r^n profile. All the others have Sérsic index n

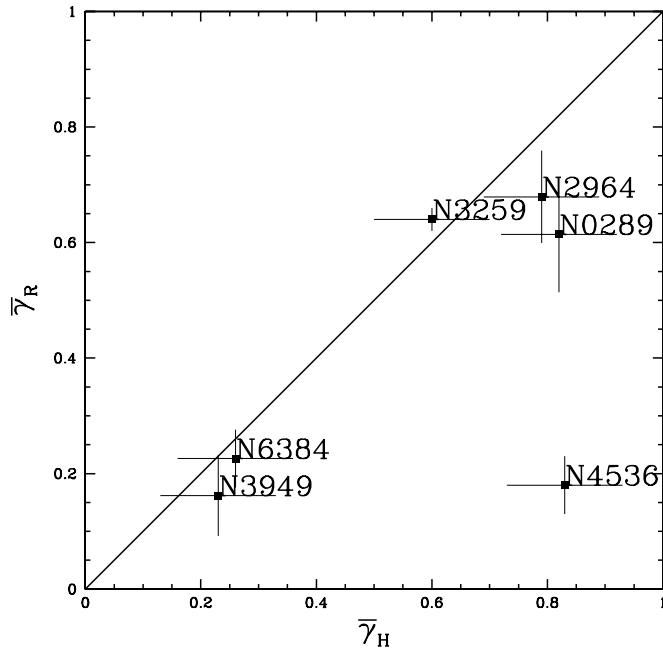


Fig. 5.—Comparison between the average logarithmic slope ($\bar{\gamma}$) measured by Seigar et al. (2002; $\bar{\gamma}_H$) from NICMOS H -band images and the values computed in this paper ($\bar{\gamma}_R$). The names of the galaxies are used to label the points. The galaxy for which $\bar{\gamma}$ is most different (NGC 4536) is strongly affected by dust in the STIS image (see Fig. 1).

consistent either with a pure exponential ($n = 1$) or with a pure $r^{1/4}$ ($n = 0.25$) profile.

In Figure 6 we show the dependence of $\bar{\gamma}$ on the absolute total V -band magnitude of the bulge (M_V) for the galaxies in our sample for which we found WFPC2 data and for which a good fit to the bulge component could be performed (*filled symbols*). We also show the objects studied in Carollo & Stiavelli (1998; *open symbols*). Squares represent bulges with an exponential profile, while circles represent the $r^{1/4}$ bulges. As previously shown in Carollo et al. (1998), we find that the two classes are well divided in the $\bar{\gamma}$ - M_V plane. The only exception is the galaxy NGC 289, for which the bulge is well described by an exponential profile but which falls in the region of the $r^{1/4}$ bulges. The results about this object are uncertain, since its morphology is strongly affected by dust extinction (the most extinguished parts of the galaxy have $\tau_{\text{eff}} \simeq 1$); furthermore, while we do not identify any distinct component in the nucleus of this galaxy, C02 suggest that a nuclear source is present. It is worth noting that the nuclear component found in C02 is defined as an uncertain detection, because of a very complex central structure.

4. PHOTOMETRICALLY DISTINCT NUCLEI

4.1. Identification and Modeling

Central, photometrically distinct, nuclear components, either resolved or not resolved, are common in galaxy nuclei (C02; Böker et al. 2002). The presence of such a component in a galaxy can often be identified by looking at the image of the galaxy itself. As an example, NGC 4041 clearly shows a bright nucleus well distinct from the galaxy disk (see Fig. 1 and Marconi et al. 2003). By looking at the SBP, these central components appear as an excess of light in the central region with respect to the best-fit model computed for each galaxy. This excess can be either of stellar nature (i.e., a nuclear stellar

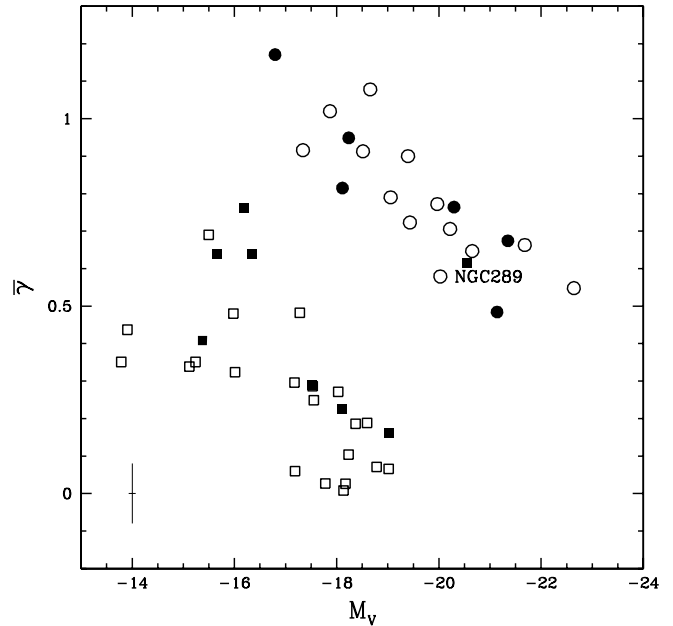


Fig. 6.—Inner cusp slope $\bar{\gamma}$ vs. V -band absolute magnitude of the bulge component. Squares and circles represent bulges with exponential and $r^{1/4}$ SBPs, respectively. The galaxies from this study are the filled symbols and those from Carollo & Stiavelli (1998) are the open symbols. From our sample only those galaxies are shown for which archival WFPC2 data were available.

cluster) or nonstellar nature (i.e., an active nucleus). In the latter case the central component is a point source and appears unresolved in the HST images. Examples of these two cases are NGC 4041, where a star cluster is present in the nucleus, and NGC 4051, which has a strong central unresolved source (see Fig. 8 in Marconi et al. 2003).

By inspecting the SBPs we identified 26 galaxies with excess light in the inner parts. Each galaxy profile was compared with the STIS PSF profile to check whether or not the nucleus was resolved. The results are shown in Table 3, where in column (2) “PS” indicates a point source and “R” indicates a resolved component. It is difficult to address the origin of the nuclear component (i.e., whether or not the light is dominated by an AGN or by stellar sources) without color and spectroscopic information. We therefore decided to be conservative and classified as star clusters only those nuclei that were well resolved at the resolution of the STIS images. With this definition the identified number of stellar clusters is a lower limit, since the appearance of a cluster (i.e., whether or not it is resolved) strongly depends on the distance of the galaxy and the instrumental resolution. We define a source to be resolved when the measured full width at half-maximum (FWHM) is $\text{FWHM} \geq 1.5 \times \text{FWHM}_{\text{PS}}$.¹⁴ Given the small field of view of the STIS images, we do not always have stars suitable to measure the point-source FWHM. We therefore used the STIS PSF created with Tiny Tim, and we measure $\text{FWHM}_{\text{PS}} = 0''.08$. Given the range of distances covered by the sample, the minimum radius that can be resolved ranges from 3 pc for the closest galaxies up to 6 pc for the most distant ones. Spectroscopic investigations of resolved nuclear sources in spiral galaxies confirm that they are generally star clusters (Böker et al. 2001; Walcher et al. 2004).

¹⁴ The value FWHM_{PS} is the FWHM of a point source.

TABLE 3
PROPERTIES OF CENTRAL COMPONENTS

Galaxy (1)	Classification (2)	M_R (mag) (3)	b (pc) (4)	FWHM (arcsec) (5)	Spectrum (6)
NGC 1255.....	PS
NGC 3021.....	R	-14.67 ± 0.3	7.7 ± 0.1	0.16	...
NGC 3162.....	R	-13.08 ± 0.6	4.1 ± 0.1	0.13	H II
NGC 3259.....	PS
NGC 3403.....	R	-9.56 ± 0.3	5.1 ± 0.5	0.13	...
NGC 3684.....	PS	H II
NGC 3686.....	PS	H II
NGC 3756.....	R	-12.10 ± 0.6	4.0 ± 0.1	0.12	H II
NGC 3887.....	R	-11.45 ± 0.6	3.8 ± 0.1	0.14	...
NGC 3949.....	PS	H II
NGC 3953.....	PS	T2
NGC 4030.....	R	-13.68 ± 0.3	6.6 ± 0.2	0.16	...
NGC 4041.....	R	-13.24 ± 0.1	14.2 ± 0.2	0.25	H II
NGC 4051.....	PS	S1.2
NGC 4100.....	R	-12.70 ± 0.1	5.1 ± 0.6	0.15	H II
NGC 4212.....	R	-13.02 ± 0.2	7.8 ± 0.4	0.19	...
NGC 4303.....	PS	H II
NGC 4321.....	R	-13.77 ± 0.1	8.8 ± 0.4	0.17	T2
NGC 4420.....	PS
NGC 4536.....	PS	H II
NGC 5054.....	R	-13.31 ± 1.3	10.8 ± 0.3	0.19	...
NGC 5364.....	R	-11.29 ± 1.4	6.6 ± 0.1	0.17	H II
NGC 5921.....	R	-14.28 ± 0.8	6.7 ± 0.1	0.15	T2
NGC 6384.....	R	-12.45 ± 1.5	8.7 ± 0.6	0.16	T2
NGC 6951.....	R	-14.63 ± 0.1	15.8 ± 0.6	0.23	S2
NGC 7314.....	PS	S1.9

NOTE.—Col. (1): Galaxy name. Col. (2): Central component classification: point source (PS) or resolved (R). Col. (3): Absolute R magnitude for resolved sources. Col. (4): Half-light radius b for resolved sources. Col. (5): Full width at half-maximum of the Gaussian used to derive b . Col. (6): Spectral classification of the nucleus from Ho et al. (1997); H II = star-forming nucleus, S = Seyfert nucleus, and T = transition object. The number attached to the class letter designates the type, except for NGC 7314 for which the classification is taken from the NASA/IPAC Extragalactic Database.

The total cluster luminosity was derived using two different techniques. In the first approach we fitted the cluster with a Gaussian function. The contribution from the underlying bulge was subtracted as a constant value given by the median galaxy flux within an annulus centered on the galaxy nucleus, with radius of $2 \times \text{FWHM}$ and thickness of 3 pixels. The total magnitude of the cluster was then obtained by the total flux under the Gaussian after the background subtraction. In the second approach, the galaxy contribution below the cluster was estimated by integrating the surface brightness of the extrapolation of the Nuker law over radii less than r_0 (see § 3). This two methods give a lower and upper limit to the cluster luminosity and therefore allow us to bracket the true cluster magnitude.

The half-light radii of the clusters were estimated from the measured Gaussian FWHM values, assuming that the intrinsic cluster profile is well described by a Plummer law:

$$I_P(r) = \frac{L}{\pi b^2} \left(1 + \frac{r^2}{b^2}\right)^{-2}. \quad (2)$$

Here L is the total luminosity and b is the half-light radius. In order to correct for the STIS instrumental width, we derived the relation between the intrinsic b and the observed FWHM by simulating 100 cluster images (with known b), convolving them with the STIS PSF, and measuring the FWHM in

the same way as done for the actual data. Tests performed to check the accuracy of these measurements showed that radii estimated in this way are accurate to within 40% (C02) for those clusters that we consider resolved ($\text{FWHM} \geq 1.5 \times \text{FWHM}_{\text{PS}}$).

The absolute total magnitudes and the corrected radii in pc are presented in Table 3, columns (3)–(4). The listed magnitudes are an average of the two estimates for the galaxies for which the Nuker fit was available to estimate the background, and the magnitudes derived with the annulus background estimate for the others. The listed uncertainties are given by the semidifference of the results with the two methods. When only the first method could be used because no Nuker fit was available for the galaxy profile, the errors were estimated by the semidifference of the magnitudes obtained by varying the annulus used to estimate the underlying galaxy contribution by ± 0.05 .

4.2. Results

We find 26 photometrically distinct components in the nuclei of our galaxies. This gives a fraction of $\simeq 55\%$, which is comparable to the fraction of $\simeq 50\%$ found by Carollo et al. (1997) in a sample of 35 spiral galaxies but smaller than the fraction of 75% found by Böker et al. (2002). However, the latter sample is mainly composed of very late type spiral galaxies (Scd or later) for which the detection of nuclear clusters

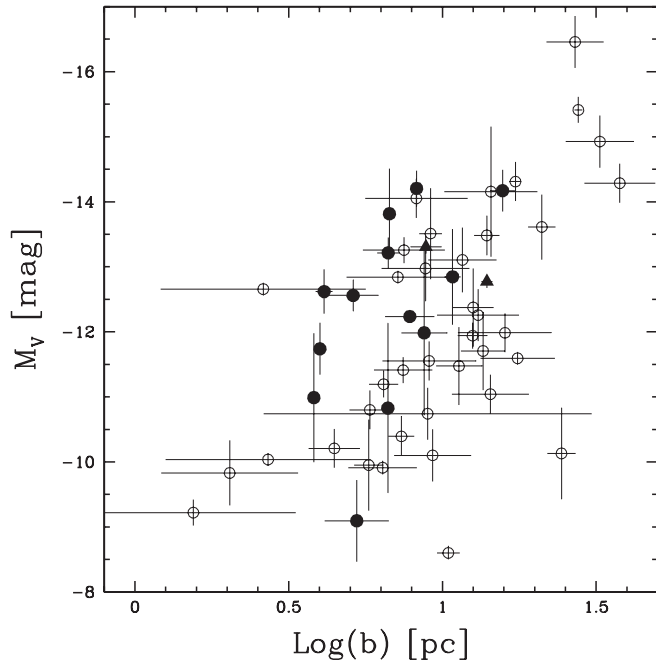


FIG. 7.—Absolute V magnitude and logarithm of the half-light radius of the nuclear clusters identified in this work (*filled circles and triangles*) and in C02 (*open circles*). Triangles represent galaxies for which we do not have the Nuker fit of the bulge component. Our sample seems to have brighter magnitudes on average for the same cluster size, especially for smaller b . This could be due to the fact that almost all our clusters are spectroscopically classified as star-forming from ground-based data (Ho et al. 1997; see text for details).

is made easier by the faintness (if not absence; Böker et al. 2003) of the bulge component.

We find that $\simeq 40\%$ of the 26 identified nuclear sources are not resolved, whereas in Carollo et al. (1997), most of the sources are resolved. This difference is probably due to the different selection criteria used to define the galaxy samples. Our sample is composed of galaxies known to have emitting gas in the nuclear regions, therefore possibly being biased to contain more active nuclei than Carollo et al.’s sample. We do not find, as in Carollo et al. (1998), that *all* the exponential bulges host a nuclear component, although one of the two cases in which the source is not detected is ambiguous: NGC 289 has a central morphology clearly affected by dust and shows a resolved nucleus in the infrared images studied by C02.

C02 present a correlation between the logarithm of the cluster size and its V -band absolute magnitude. They find that this correlation exists also in the H -band data, in which the extinction by dust is less important than in the STIS data ($A_H/A_R = 0.25$; Cardelli et al. 1989). For our sample of clusters we find the same correlation with a linear correlation coefficient of -0.52 (significance level greater than 95%). However, the correlation disappears when we properly account for the mutual dependence of the two variables on distance. Indeed, using a partial correlation analysis (Fisher 1990), we find that the significance level of the correlation between the magnitude and the radius decreases to 62.16% (while still significant for the C02 sample). This phenomenon is probably due to the small size of our sample (15 objects, compared with 38 identified by C02 in F606W). However, it can also be due to the fact that we are sampling a smaller range in distances. The comparison with the C02 sample of nuclear

clusters is shown in Figure 7. Nuclear star clusters identified in this work are represented as filled circles and triangles, while the C02 sample is shown with open circles. Triangles represent galaxies for which we do not have the Nuker fit of the bulge component. Our sample seems to have brighter magnitudes for the same cluster size, the discrepancy being larger for smaller radii. This can be due to the fact that almost all galaxy nuclei hosting clusters are spectroscopically classified as star-forming (H II region-type spectrum) from ground-based data (Ho et al. 1997). Indeed, Carollo et al. (1997) already noted that the central sources in star-forming galaxies are typically brighter than those in non-star-forming galaxies, for similar radii.

5. DISCUSSION AND CONCLUSIONS

We analyzed optical images of the central regions of 48 nearby spiral galaxies (44 Sbc and 4 Sc). The extracted SBPs were modeled with a Nuker law, and the average logarithmic slope was computed for each best-fit model. For a subsample of 15 objects we extracted the SBP from WFPC2 images, and we derived the bulge properties by fitting an exponential, an $r^{1/4}$, or a Sérsic profile.

In agreement with earlier studies, we find that galaxy bulges divide into two classes, on the basis of their $\bar{\gamma}$ and bulge SBP. In our sample of 15 Sbc spiral galaxies we find that $\sim 50\%$ of bulges are exponential, and the other half are $r^{1/4}$. This fraction is higher than the fraction of $r^{1/4}$ bulges found by Carollo & Stiavelli (1998) and is more consistent with the fraction of $r^{1/4}$ bulges found in S0–Sab galaxies. We also tried to fit the bulge SBP with an r^n law, but the fitted n -values were generally found to be consistent with a pure exponential ($n = 1$) or pure $r^{1/4}$ ($n = 0.25$) profile, implying no need for using a more general Sérsic law. Only one galaxy is best fitted with a Sérsic profile, with index $n = 0.5$. This result contrasts with a recent study by Balcells et al. (2003) of 19 spiral galaxies (from S0 to Sbc morphological type), in which they find no galaxies with an $r^{1/4}$ bulge. From their Figure 2, we deduce that they fitted all the Sbc galaxies with a pure exponential profile, but their sample contains only four Sbc spiral galaxies. Therefore, any conclusion about the lack of $r^{1/4}$ bulges in this morphological class is doubtful.

We find that $\sim 55\%$ of our galaxies have a nuclear component and about half of them are resolved. Because of the lack of color and spectral information, it is difficult to address the origin of the nuclei. We conservatively decided to classify as star clusters (rather than AGNs) only those nuclei that were well resolved at the *HST* resolution. We found 15 nuclear clusters, with absolute magnitudes ranging from -10 up to -14.5 . The identified clusters are, on average, brighter than those previously found. This might be due to a bias in our sample toward star-forming galaxies, combined with a trend for star-forming nuclei to host brighter central clusters.

This work was funded by NASA grants for program GO-8228 from the Space Telescope Science Institute (operated by the Association of Universities for Research in Astronomy, Inc., under NASA contract NAS 5-26555). We made use of the NASA/IPAC Extragalactic Database, which is operated by the Jet Propulsion Laboratory, California Institute of Technology, under contract with NASA.

REFERENCES

- Balcells, M., Graham, A. W., Domínguez-Palmero, L., & Peletier, R. F. 2003, *ApJ*, 582, L79
- Bevington, P. R., & Robinson, D. K. 1992, *Data Reduction and Error Analysis for the Physical Sciences* (2nd ed.; New York: McGraw-Hill)
- Böker, T., Laine, S., van der Marel, R. P., Sarzi, M., Rix, H., Ho, L. C., & Shields, J. C. 2002, *AJ*, 123, 1389
- Böker, T., Stanek, R., & van der Marel, R. P. 2003, *AJ*, 125, 1073
- Böker, T., van der Marel, R. P., Mazzuca, L., Rix, H.-W., Rudnick, G., Ho, L. C., & Shields, J. C. 2001, *AJ*, 121, 1473
- Cardelli, J. A., Clayton, G. C., & Mathis, J. S. 1989, *ApJ*, 345, 245
- Carollo, C. M. 1999, *ApJ*, 523, 566
- Carollo, C. M., & Stiavelli, M. 1998, *AJ*, 115, 2306
- Carollo, C. M., Stiavelli, M., de Zeeuw, P. T., & Mack, J. 1997, *AJ*, 114, 2366
- Carollo, C. M., Stiavelli, M., & Mack, J. 1998, *AJ*, 116, 68
- Carollo, C. M., Stiavelli, M., Seigar, M., de Zeeuw, P. T., & Dejonghe, H. 2002, *AJ*, 123, 159 (C02)
- de Vaucouleurs, G., de Vaucouleurs, A., Corwin, H. G., Jr., Buta, R. J., Paturel, G., & Fouqué, P. 1991, *Third Reference Catalogue of Bright Galaxies* (New York: Springer)
- Ferrarese, L., & Merritt, D. 2000, *ApJ*, 539, L9
- Ferrarese, L., van den Bosch, F. C., Ford, H. C., Jaffe, W., & O'Connell, R. W. 1994, *AJ*, 108, 1598
- Fisher, R. A. 1990, *Statistical Methods, Experimental Design, and Scientific Inference* (Oxford: Oxford Univ. Press)
- Forbes, D. A., Franx, M., & Illingworth, G. D. 1995, *AJ*, 109, 1988
- Freeman, K. C. 1970, *ApJ*, 160, 811
- Gebhardt, K., et al. 2000, *ApJ*, 539, L13
- Haehnelt, M. G., & Kauffmann, G. 2000, *MNRAS*, 318, L35
- Ho, L. C., Filippenko, A. V., & Sargent, W. L. W. 1997, *ApJ*, 487, 579
- Holtzman, J. A., Burrows, C. J., Casertano, S., Hester, J. J., Trauger, J. T., Watson, A. M., & Worthey, G. 1995, *PASP*, 107, 1065
- Hughes, M. A., et al. 2003, *AJ*, 126, 742
- . 2004, in preparation
- Kinney, A. L., Calzetti, D., Bohlin, R. C., McQuade, K., Storchi-Bergmann, T., & Schmitt, H. R. 1996, *ApJ*, 467, 38
- Kormendy, J. 1993, in *IAU Symp. 153, Galactic Bulges*, ed. H. Dejonghe & H. J. Habing (Dordrecht: Kluwer), 209
- Kormendy, J., & Gebhardt, K. 2001, *AIP Conf. Proc. 586, 20th Texas Symposium on Relativistic Astrophysics*, ed. J. C. Wheeler & H. Martel (New York: AIP), 363
- Krist, J., & Hook, R. 2001, *The Tiny Tim User's Guide*, Version 6.0 (Baltimore: STScI)
- Laine, S., van der Marel, R. P., Lauer, T. R., Postman, M., O'Dea, C. P., & Owen, F. N. 2003, *AJ*, 125, 478
- Lauer, T. R., et al. 1995, *AJ*, 110, 2622
- Magorrian, J., et al. 1998, *AJ*, 115, 2285
- Marconi, A., et al. 2003, *ApJ*, 586, 868
- Marconi, A., & Hunt, L. K. 2003, *ApJ*, 589, L21
- Merritt, D., & Ferrarese, L. 2001, *ApJ*, 547, 140
- Norman, C. A., Sellwood, J. A., & Hasan, H. 1996, *ApJ*, 462, 114
- Oke, J. B. 1974, *ApJS*, 27, 21
- Paturel, G., Petit, C., Prugniel, P., Theureau, G., Rousseau, J., Brouty, M., Dubois, P., & Cambrésy, L. 2003, *A&A*, 412, 45
- Proffitt, C., et al. 2002, *STIS Instrument Handbook*, Version 6.0 (Baltimore: STScI)
- Ravindranath, S., Ho, L. C., Peng, C. Y., Filippenko, A. V., & Sargent, W. L. 2001, *AJ*, 122, 653
- Schlegel, D. J., Finkbeiner, D. P., & Davis, M. 1998, *ApJ*, 500, 525
- Seigar, M., Carollo, C. M., Stiavelli, M., de Zeeuw, P. T., & Dejonghe, H. 2002, *AJ*, 123, 184
- Sérsic, J. -L. 1968, *Atlas de Galaxias Australes* (Córdoba: Obs. Astron., Univ. Nac. Córdoba)
- Silk, J., & Rees, M. J. 1998, *A&A*, 331, L1
- Stiavelli, M., Miller, B. W., Ferguson, H. C., Mack, J., Whitmore, B. C., & Lotz, J. M. 2001, *AJ*, 121, 1385
- Walcher, C. J., Häring, N., Böker, T., Rix, H.-W., van der Marel, R. P., Gerssen, J., Ho, L. C., & Shields, J. C. 2004, in *Coevolution of Black Holes and Galaxies*, ed. L. C. Ho (Pasadena: Carnegie Obs.), <http://www.ociw.edu/ociw/symposia/series/symposium1/proceedings.html>
- Witt, A. N., Petersohn, J. K., Bohlin, R. C., O'Connell, R. W., Roberts, M. S., Smith, A. M., & Stecher, T. P. 1992, *ApJ*, 395, L5